Research Article
Molecular and Cell Biology

JOURNAL
OF HEPATOLOGY

Generation of hepatobiliary organoids from human induced pluripotent stem cells

Graphical abstract

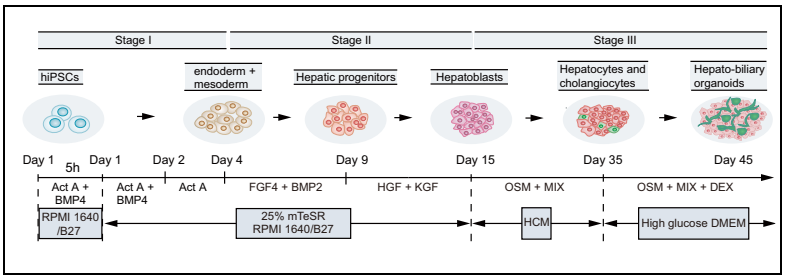

Highlights

- We established a system to generate hiPSC-derived hepatobiliary organoids *in vitro.*
- To varying degrees, this model recapitulated several key aspects of hepatobiliary organogenesis.
- The hepatobiliary organoids displayed a series of hepatic and biliary functional attributes.
- This system does not rely on any exogenous cells or genetic manipulation.

Authors

Fenfang Wu, Di Wu, Yong Ren, ...,
Xiaoni Chen, Shangwu Chen, Anlong Xu

Correspondence

lssxal@mail.sysu.edu.cn (A. Xu)

Lay summary

Herein, we established a system to generate human induced pluripotent stem cell-derived functional hepatobiliary organoids *in vitro,* without any exogenous cells or genetic manipulation. To some extent this model was able to recapitulate several key aspects of hepatobiliary organogenesis in a parallel fashion, holding great promise for drug development and liver transplantation.

http://dx.doi.org/10.1016/j.jhep.2018.12.028
 J. Hepatol. 2019, 70, 1145–1158

Research Article
Molecular and Cell Biology

JOURNAL OF HEPATOLOGY

Generation of hepatobiliary organoids from human induced pluripotent stem cells

Fenfang Wu[1,†], Di Wu[1,†], Yong Ren[1,†], Yuhua Huang[1], Bo Feng[1], Nan Zhao[1], Taotao Zhang[1], Xiaoni Chen[1], Shangwu Chen[1], Anlong Xu[1,2,*]

[1]*State Key Laboratory of Biocontrol, Guangdong Province Key Laboratory for Pharmaceutical Functional Genes, College of Life Sciences, Sun Yat-Sen University, Guangzhou, Guangdong 510006, People's Republic of China;* [2]*School of Life Science, Beijing University of Chinese Medicine, Beijing 100029, People's Republic of China*

Background & Aims: Human induced pluripotent stem cell (hiPSC)-derived liver modeling systems have the potential to overcome the shortage of donors for clinical application and become a model for drug development. Although several strategies are available to generate hepatic micro-tissues, few have succeeded in generating a liver organoid with hepatobiliary structure from hiPSCs.

Methods: At differentiation stages I and II (day 1–15), 25% of mTeSR™ culture medium was added to hepatic differentiation medium to induce endodermal and mesodermal commitment and thereafter hepatic and biliary co-differentiation. At stage III (day 15–45), 10% cholesterol$^+$ MIX was added to the maturation medium to promote the formation and maturation of the hepatobiliary organoids. Phenotypes and functions of organoids were determined by specific markers and multiple functional assays both *in vitro* and *in vivo*.

Results: In this system, hiPSCs were induced to form 3D hepatobiliary organoids and to some extent recapitulated key aspects of early hepatogenesis in a parallel fashion. The organoids displayed a series of functional attributes. Specifically, the induced hepatocyte-like cells could take up indocyanine green, accumulate lipid and glycogen, and displayed appropriate secretion ability (albumin and urea) and drug metabolic ability (CYP3A4 activity and inducibility); the biliary structures in the system showed gamma glutamyltransferase activity and the ability to efflux rhodamine and store bile acids. Furthermore, after transplantation into the immune-deficient mice, the organoids survived for more than 8 weeks.

Conclusion: This is the first time that functional hepatobiliary organoids have been generated from hiPSCs. The organoid model will be useful for *in vitro* studies of the molecular mechanisms of liver development and has important potential in the therapy of liver diseases.

Lay summary: Herein, we established a system to generate human induced pluripotent stem cell-derived functional hepatobiliary organoids *in vitro*, without any exogenous cells or genetic manipulation. To some extent this model was able to recapitulate several key aspects of hepatobiliary organogenesis in a parallel fashion, holding great promise for drug development and liver transplantation.

Introduction

To date, most of the pluripotent stem cell (PSC)-based liver modeling systems have initiated differentiation from highly purified definitive endoderm (DE) and have generated monolayer hepatocyte-like cells.[1–5] However, preclinical predictions from such models are usually difficult to interpret, and may be misleading, because homogeneous DE populations are insufficient to accurately replicate the complex regulation of signals among cells and tissues during liver organogenesis.[6] A recent study, which mimicked liver development by combining hepatic endoderm cells with endothelial cells and mesenchymal progenitors, resulted in the generation of a liver bud-like structure with improved function.[7] Similarly, co-culture of fetal liver progenitor cells and liver extracellular matrix triggered the formation of hepatocytes with bile duct-like structures.[8] These findings highlighted the importance of multicellular interactions during early liver development. However, these studies combined cells that were isolated from multiple and postnatal individuals, suggesting a severe limitation of the transplanting applications based on these strategies.

Here, we reported a method to generate functional hepatobiliary organoids (HBOs) from hiPSCs. To achieve this goal, we learned from early hepatogenesis and simultaneously induced endoderm and a small part of mesoderm by the inclusion of 25% mTeSR into hepatic differentiation medium. This treatment mildly suppressed/delayed early hepatic differentiation, but turned on biliary specification by activating the NOTCH2 and TGF-β signaling pathway. Then we achieved co-differentiation of hepatocyte-like cells and cholangiocyte-like cells. Finally, our uniquely prepared cholesterol$^+$ MIX (mainly comprised of cholesterol and other small molecules) promoted the HBO formation and functional maturation.

Keywords: hiPSC; Differentiation; Hepatobiliary organoids; Organogenesis.
Received 15 April 2018; received in revised form 28 November 2018; accepted 19 December 2018; available online 7 January 2019

* Corresponding author. Address: State Key Laboratory of Biocontrol, Guangdong Province Key Laboratory for Pharmaceutical Functional Genes, College of Life Sciences, Sun Yat-Sen University, Guangzhou, Guangdong 510006, People's Republic of China. Tel.: +86 20 39332990; fax: +86 20 39332950.
E-mail address: lssxal@mail.sysu.edu.cn (A. Xu).
† These authors contributed equally to this work.

Materials and methods

Cell culture

Human-induced PSC (hiPSC) lines UC and WD were obtained from Guangzhou Institutes of Biomedicine and Health, Chinese Academy of Science. The passage numbers of the 2 cell lines ranged from 20 to 40. Human ESC line H1 was obtained from Wisconsin Cell Research Institute. The passage number of the H1 cells used here ranged from 44 to 60. All 3 cell lines were cultured on Matrigel (BD Biosciences)-coated plates and maintained in mTeSR™ medium (STEMCELL Technologies). Cryopreserved adult human hepatocytes were purchased from Lonza and used for further analysis after 48 h in hepatocyte culture medium (HCM) (Lonza). The HepG2 cells (from our own lab) were cultured in HCM.

Differentiation of hepatobiliary organoids

Before the initiation of hepatobiliary differentiation, PSCs were dissociated into clumps using Dispase (Sigma-Aldrich), and were plated onto Matrigel Basement Membrane Matrix Growth Factor Reduced (BD Biosciences). When the cells attained a confluence of 80–90% (depending on the cell line), mTeSR was replaced with RPMI1640/B27 minus insulin (Gibco) containing 100 ng/ml Activin A and 20 ng/ml BMP4 (Peprotech) for 5 h. The medium was then replaced with RPMI1640/B27 containing 25% mTeSR, 100 ng/ml Activin A and 20 ng/ml BMP4 for 2 days, followed by RPMI1640/B27 containing 100 ng/ml Activin A, and cultured for another 2 days. Next, the cultures were placed in RPMI1640/B27 containing 25% mTeSR, 30 ng/ml FGF4 and 20 ng/ml BMP2 (Peprotech) for 5 days, and in RPMI1640/B27 containing 25% mTeSR, 20 ng/ml HGF and 20 ng/ml KGF (both from Peprotech) and cultured for a further 6 days. Finally, the differentiated cells were cultured in HCM supplemented with 10 ng/ml oncostatin M (OSM) (R&D System) and 0.1 μM dexamethasone (Dex) (Sigma-Aldrich) with or without 10% cholesterol$^+$ MIX for 20 days. Subsequently, cells were cultured in high glucose DMEM (Gibco) containing ascorbic acid (1:1,000), fatty acid free bovine serum albumin (1:500), transferrin (1:1,000), insulin (1:1,000), gentamicin/amphotericin-B (1:1,000) (Lonza), 10 ng/ml OSM with or without 10% cholesterol$^+$ MIX for further culture. Medium was changed every 24 h. The differentiation protocol and sequential morphological changes are illustrated in Fig. 1.

Inhibition of signaling

To inhibit NOTCH/VEGFR/TGF-β signaling, DAPT (10 mM)/SU11248 (1 μM)/SB431542 (10 μM) (all from APExBIO) was included into the medium of mTeSR$^+$ group throughout the differentiation period on a daily basis. The mTeSR withdrawal was performed from day 9. All relevant assays were performed using the day-25 cultures that were exposed to different treatments.

Cholesterol$^+$ MIX preparation

Cholesterol$^+$ MIX is a patent pending product (Chinese pending patent number: ZL 201810211144.X) developed from our own lab, which can be ordered from ProbeChem, and is mainly comprised of cholesterol and other small molecules (see Fig. S2) uniquely prepared from Chinese medicine products. And 10% cholesterol$^+$ MIX was used to promote hepatic and biliary maturation in our system.

RNA extraction and quantitative PCR

Total RNAs were isolated with TRIzol Reagent (Thermo Scientific). Total RNAs of human fetal liver and human adult liver were purchased from Clonetech. Total RNA of human intrahepatic biliary epithelial cells total RNA was purchased from ScienCell. The cDNA was synthesized with 500 ng of total RNA using PrimeScript RT reagent Kit with gDNA Eraser (TAKARA). Quantitative PCR was performed with TB Green Premix Ex Taq II (TAKARA) using the LightCycler 480 II (Roche). Relative quantification was performed against a standard curve and the values were normalized against the housekeeping gene, glyceraldehyde 3-phosphate dehydrogenase (GAPDH). Primers used are listed (Table S1).

Microarray analysis

Total RNAs were isolated using the RNeasy Mini Kit (Qiagen). RNA purity was checked using the NanoPhotometer®

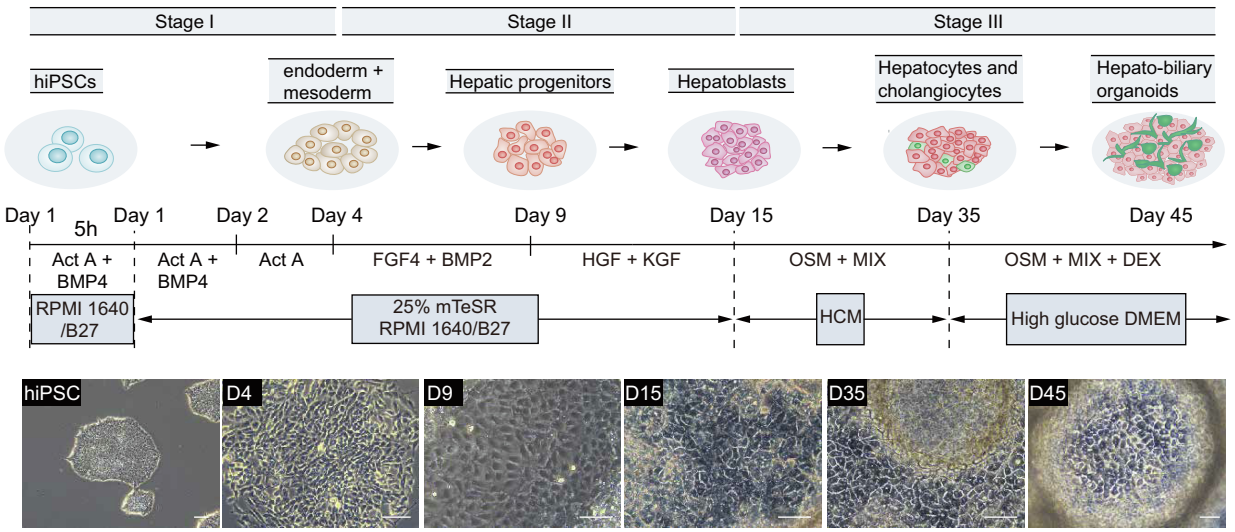

Fig. 1. Generation of hepatobiliary organoids from hiPSCs. (A) Schematic representation of the differentiation procedure. (B) Sequential morphological changes (day 0–45) of hiPSC differentiation into hepatobiliary organoids. Scale bars = 50 μm. hiPSCs, human induced pluripotent stem cells. (This figure appears in colour on the web.)

spectrophotometer (IMPLEN), and the integrity was assessed using the RNA Nano 6000 Assay Kit of the Agilent Bioanalyzer 2100 system (Agilent Technologies). Total 1.5 μg RNAs per sample were used as the input material for the RNA sample preparations. Sequencing libraries were generated using NEBNext® Ultra RNA Library Prep Kit for Illumina® (NEB) in accordance with the manufacturer's recommendations. Index codes were added to attribute sequences to each sample. The clustering of the index-coded samples was performed on a cBot Cluster Generation System using TruSeq PE Cluster Kit v3-cBot-HS (Illumina) according to the manufacturer's instructions. After cluster generation, the library preparations were sequenced on an Illumina Hiseq platform and paired-end reads were generated. Differential expression analyses of the 2 groups were performed using the DESeq R package. The resulting *p* values were adjusted using the Benjamini and Hochberg's approach for controlling the false discovery rate. Genes with an adjusted *p* value <0.05 determined by DESeq were considered as differentially expressed.

Immunofluorescence

Monolayer staining: monolayer cells were fixed with 4% paraformaldehyde (PFA) for 20 min at room temperature (RT), and permeabilized with 0.2% Triton X-100 (Sigma-Aldrich) or cold 100% methanol. After blocking with 10% donkey serum (The Jackson Laboratory) for 1 h, the cells were incubated with primary antibodies in 1% donkey serum at 4 °C overnight, and secondary antibodies in 1% donkey serum for 45 min at RT. Finally, DAPI (Sigma-Aldrich) was used to counterstain the nuclei. Samples were washed 4 times with PBS for 5 min at RT after primary and secondary antibody and DAPI staining.

The 3D structure staining was performed as follows: 3D samples were fixed with 4% PFA at RT overnight, washed with normal saline (0.85% NaCl) and then embedded in Richard-Allan Scientific HistoGel (Thermo Scientific). The HistoGel block was dehydrated, embedded in paraffin and sectioned at 4 μm. Paraffin-embedded sections were dewaxed with xylene, rehydrated, placed in Tris-EGTA-buffer (pH 9.0) or citrate buffer (pH 6.0) and subjected to heat mediated antigen retrieval (Microwave) for 20 min. The subsequent staining steps are described above (as per monolayer staining).

All immunofluorescence images were acquired using a Leica TCS-SP5 confocal microscope. LAS X software (Leica) was used for image processing. A complete list of the primary and secondary antibodies used is provided (Table S2).

Flow cytometry

Samples were incubated with TrypLE (Gibco) at 37 °C until the cells began to dissociate. Cells were centrifuged and resuspended in 2% PFA at 4 °C for 20 min and centrifuged and resuspended in flow cytometry buffer (PBS, 5% FBS, 0.1% Triton X-100). Cells were then incubated with primary antibodies or control IgGs for 30 min on ice, and secondary antibodies for 20 min on ice. Analysis was performed using a FACS LSR Fortessa flow cytometer (BD Biosciences). IgG controls were used to set gates for positive cells. All antibodies are listed (Table S3).

Senescence β-Gal staining

The cultures were fixed in the 4% PFA for 15 min at RT, then β-Gal staining (Cell Signal) was performed in accordance with the manufacturer's instructions.

Periodic acid-Schiff and Oil Red-O staining

Periodic acid-Schiff (PAS) (Polysciences) and Oil Red-O (ORO) (Sigma-Aldrich) staining were performed in accordance with the manufacturer's instructions.

Cellular uptake and release of indocyanine green

The cultures were incubated with 1 mg/ml indocyanine green (ICG) (Sigma-Aldrich) for 30 min at 37 °C, the medium containing ICG was discarded and the cells washed with PBS. Then cellular uptake of ICG was examined under the microscopy. Cells were then returned to the culture medium and incubated for a further 12 h to determine the release of cellular ICG.

Alpha-fetoprotein, albumin and urea assay

Human alpha-fetoprotein (AFP) and albumin production were detected using ELISA kits (Bethyl Laboratories). Urea production was detected using the Quantichrom Urea assay Kit (Bioassay Systems). Cells were incubated in fresh medium for 24 h and subsequently the cell supernatant was collected at different time points and analyzed for albumin secretion. Cells were either trypsinized and counted using a hemocytometer, or lysed for protein content assay with a BCA Protein Assay Kit (Thermo Scientific).

CYP3A4 activity and inductivity

CYP3A4 activity was measured using Luminescence-based assays (Promega). Briefly, the organoids, cryopreserved adult hepatocytes (Lonza) and HepG2 cells (ATCC) were rinsed in HCM and incubated with the luminescent substrate (luciferin-IPA) and then cells were diluted in the same medium for 1 h (3 mM luciferin-IPA) at 37 °C. Following incubation, supernatants were processed in accordance with the manufacturer's instructions. Luminescence was measured using a luminometer (GloMax Discover, Promega).

For CYP3A4 induction assays, cultures were treated with rifampin (25 mM) or phenobarbital (1 mM) or 0.1% vol/vol DMSO control (Sigma-Aldrich) dissolved in HCM for 72 h, followed by quantification of CYP3A4 activity using the luminescent assays described above. Inducer compounds were replaced daily.

Rhodamine transport assay

The cysts were incubated with 100 μM rhodamine 123 (Sigma-Aldrich) for 5 min at 37 °C and then washed 3 times with cell culture medium. Fresh differentiation medium was added following the third wash. The organoids were incubated at 37 °C for another 40 min. To demonstrate that rhodamine 123 transfer indeed reflected the activity of the membrane channel multidrug resistance protein 1 (MDR1), cysts were further incubated with 10 μM verapamil (Sigma-Aldrich) at 37 °C for 30 min and the rhodamine assay was repeated. Following completion of each experiment, images were taken using a Leica TCS-SP5 confocal microscope. LAS X software (Leica) was used for image processing.

Measurement of GGT activity

Gamma-glutamyltransferase (GGT) activity was measured in triplicate using the MaxDiscovery GGT Enzymatic Assay Kit (Bio Scientific) in accordance with the manufacturer's instructions. Substrate only was used as the negative control.

Analysis of bile acids by LC-MS/MS

Briefly, cystic organoids were washed in cold PBS and punctured using a microsyringe. The liquid in the cystic structures was then aspirated under the microscope and diluted with 50% methanol for LC-MS/MS analysis. The samples were stored at −20 °C.

For each sample, 20 μl of a 50 μM cholic acid (in methanol) was added to 60 μl of the diluted sample. Methanol was used as an internal standard. The mixture was deproteinized by the addition of 200 μl of acetonitrile. Each sample was vortexed for 10 s and centrifuged at 14,000*g* at 4 °C for 5 min. The supernatant was transferred to a new glass tube and extracted with 2 ml of a mixture of ethyl acetate and t-butyl methyl ether (2:1). After centrifugation at 3,000*g* at 4 °C for 15 min, the organic phase was transferred to a new glass tube and evaporated under a stream of nitrogen gas. The residue was reconstituted in 60 μl of 50% methanol solution containing 0.2% formic acid. Ten microliters of each reconstituted sample were injected into a liquid chromatography tandem mass spectrometry (LC-MS/MS) for analysis.

LC-MS/MS analysis was performed on each sample using an API 2000 Mass Spectrometer (SCIEX) equipped with a Shimadzu HPLC LC-20 AD (Shimadzu). A Phenomenex Luna C18 analytical column (3 μm, 100 mm × 2 mm inner diameter column) (Torrance) was used to separate free bile acids. The flow rate through the column, conducted at ambient temperature was 0.2 ml/min, and optimal resolution was achieved by elution with a linear gradient of water containing 0.1% formic acid (45%→0%) and methanol (55%→100%) for 10 min at RT. The mass spectrometer was operated in the turbo ion spray mode with positive ion detection. The turbo ion spray temperature was maintained at 350 °C, and a voltage of 4.8 kV was applied to the sprayer needle. The detection and quantification of free and conjugated bile acids and the internal standard were accomplished by multiple reaction monitoring with the transition m/z 403.3/367.4 for dehydrocholic acid, 359.1/135.0 for lithocholic acid, 375.1/357.2 for free deoxycholic acid, chenodeoxycholic acid, hyodeoxycholic acid, ursodeoxycholic acid, and murideoxycholic acid, 373.1/355.3 for free cholic acid, hyocholic acid, α- and ω-muricholic acid (MCA), and 391.1/355.2 for β-MCA.

Transplantation assay

Animal experiments were performed in accordance with the framework of the Institutional Animal Care and Use Committee of Sun Yat-sen University. Six- to eight-week-old female NOD-SCID mice, weight between 20–25 g (purchased from BIOCYTOGEN) were used as recipients. These mice were kept in individually ventilated cages under controlled light conditions (26 °C, 12 h light/12 h darkness cycle) and the mice were allowed free access to water and a dry pellet diet. Before performing the operations, mice were anesthetized with pentobarbital sodium (Sigma-Aldrich) with a dosage of 35 mg/kg. The operation group (20 mice) were anesthetized with pentobarbital sodium (Sigma-Aldrich) with a dosage of 35 mg/kg. HBOs matured *in vitro* for 45 days were carefully removed from the dish using tweezers, washed with cold PBS and then transplanted under the splenic capsules of the mice. Briefly, a small left-lateral peritoneal layer incision was made to expose the spleen, a subcapsular pocket was created and the organoids were placed into the pocket. The spleen was then returned to the peritoneal cavity and the skin was closed in a double layer. For the sham operation group (6 mice), the manipulation was performed as per the operation group with the exception of the organoid transplantations. At 8 weeks following engraftment, the mice were humanely euthanized and subjected to further experimentation. No formal randomization method was used to assign animals to study groups. However, littermate animals from a given cage were randomly assigned to experimental or control groups by a technician not involved in the study. Blinding was not performed.

Statistical analyses

All statistical analyses were performed using GraphPad Prism 7.04. For comparison between 2 mean values, a 2-sided Student's *t* test was used to calculate statistical significance.

Results

Our 3-stage approach to generate hiPSC-derived HBOs, and sequential morphological changes is outlined in Fig. 1A and B.

Differentiation of hiPSCs into endoderm and mesoderm

Before differentiation, we examined the pluripotency of hiPSCs at day 0 by immunofluorescence and found that more than 90% of cells co-expressed OCT4 and NANOG (Fig. 2A). This result was confirmed by flow cytometry (Fig. 2B). For stage I, we hypothesized that by retaining a certain proportion of mTeSR in the hepatic differentiation medium we might be able to promote endoderm formation accompanied by a small portion of mesoderm, and thereafter hepatobiliary commitment. This hypothesis was based on the knowledge of several growth factors in mTeSR (FGF2, TGF-β and LiCl):[9] (i) FGF2 can switch BMP4-induced hPSC differentiation outcome to mesendoderm;[10] (ii) TGF-β plays a role in hepatic fate determination[11–12] and is required *in vivo* for biliary specification; (iii) Lithium-induced WNT activation[13] may contribute to hepatic endoderm.[14] We initially treated hiPSCs with DE medium that contained various ratios of mTeSR (25% or 50% or 75%). However, none of these conditions showed sufficient endodermal commitment by day 4, as determined by the low numbers of FOXA2-positive cells (data not shown). We reasoned that the growth factor mediated effect might be hindered by mTeSR.

Thus, we modified the protocol by giving a 5 h-prestimulation using DE medium only, and sequentially supplemented DE medium with mTeSR over a 4-day period (Fig. 1A). As a result, the cells with 25% mTeSR treatment showed robust upregulation of genes associated with endoderm (*FOXA2*, *SOX17*, *GATA4* and *GATA6*) and mesoderm (*BRA*, *EMOS* and *MIXL1*), along with the downregulation of genes associated with non-neural ectoderm (*DLX3*), neuroectoderm (*SOX1*), trophoblast (*CDX2*) and pluripotency (*OCT4* and *NANOG*) (Fig. 2C). Immunofluorescence at day 4 showed that more than 70% of cells co-expressed DE markers FOXA2 and SOX17, about 20% of cells expressed mesoderm marker BRA, whereas very few cells expressed ectoderm marker NESTIN (Fig. 2D). Flow cytometry further confirmed the ratio of endodermal and mesodermal lineages (Fig. 2E). These results indicated that such sequential treatments can lead to successful differentiation of hiPSCs into DE concomitantly with mesodermal fate. Other concentrations of mTeSR were not used because of the poor efficacy in DE induction (Fig. S1).

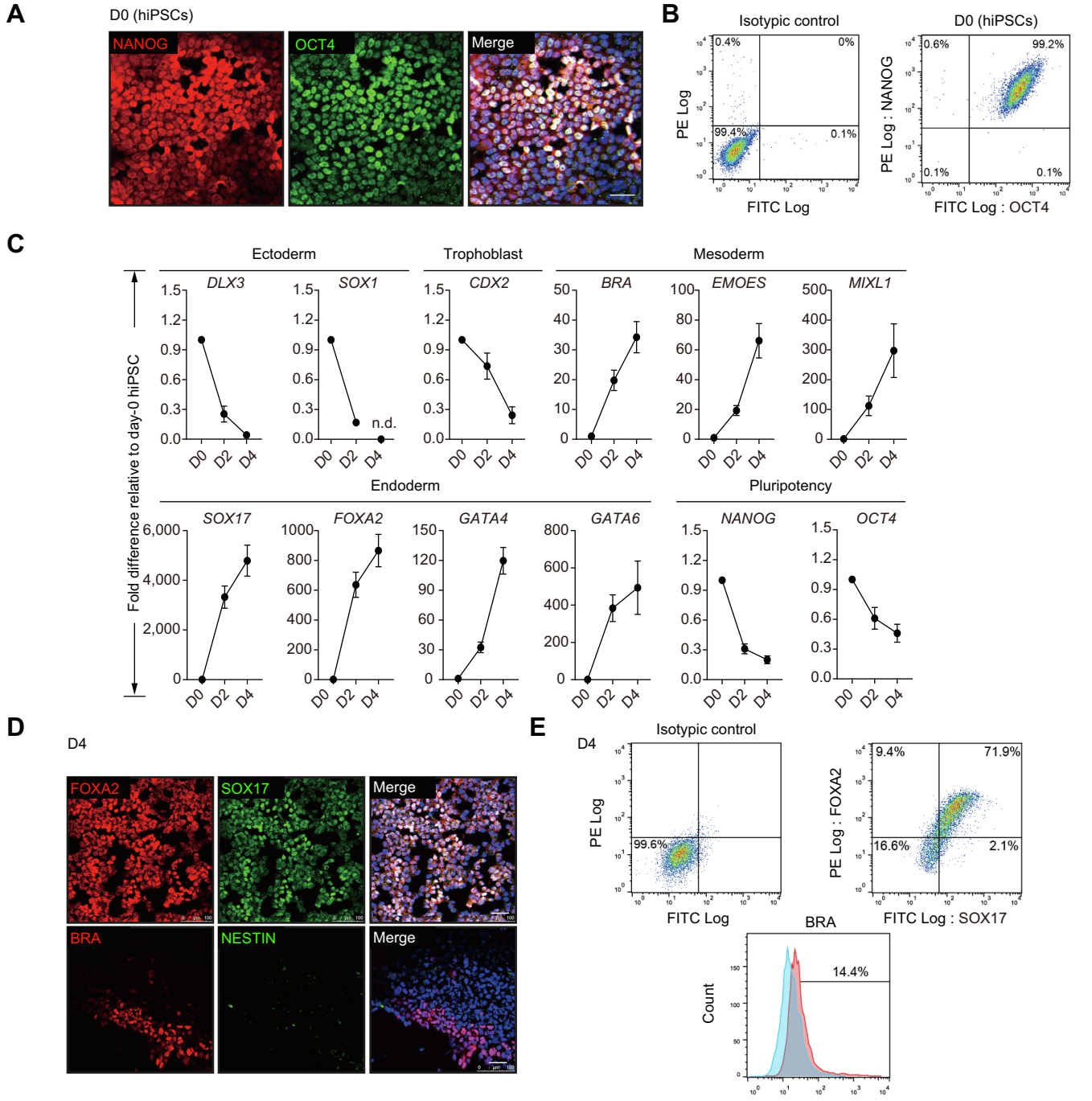

Fig. 2. Differentiation of hiPSCs into endoderm and a small part of mesoderm. (A) Immunofluorescence showed the co-expression of NANOG and OCT4 in most day 0 hiPSCs. (B) Flow cytometry confirmed that most day 0 hiPSCs were NANOG positive and OCT4 positive. (C) Quantitative PCR analysis (D) Immunofluorescence and (E) Flow cytometry showed that inclusion of 25% mTeSR into the endoderm medium resulted in main endoderm and a small part mesoderm commitment. In (C), values are determined relative to *GAPDH* and presented as fold change relative to the expression in day 0 hiPSCs, which is set as 1. n = 3. All scale bars = 50 μm. All error bars indicate ± s.d. hiPSCs, human induced pluripotent stem cells. (This figure appears in colour on the web.)

Hepatic and biliary co-differentiation

For stage II, FGF4 plus BMP2 and HGF plus KGF were used in sequence to induce and expand the hepatoblasts based on *in vivo* developmental cues.[15–18] A total of 25% mTeSR was maintained until the maturation stage (referred to MT^+ group), given the possible role of mTeSR in promoting hepatic and biliary differentiation as described above. The hiPSC-derived hepatocyte-like cells that without mTeSR treatment were induced in parallel and used as control (MT^- group).

Formation of liver-buds depends on transient expression of Tbx3.[19] As the liver bud expands, progenitor cells downregulate Tbx3 and maintain and/or upregulate the expression of hepatic and biliary genes.[20] Compared with the MT^- group, the MT^+ group also showed transient, although weaker, upregulation of *TBX3*, with the peak level at day 9, and persistent upregulation of *HNF4α* and *AFP*, thus identifying this time as the stage of hepatic specification (Fig. 3A). Approximately 70% of cells at day 9 co-expressed HNF4α and AFP as shown by immunofluorescence

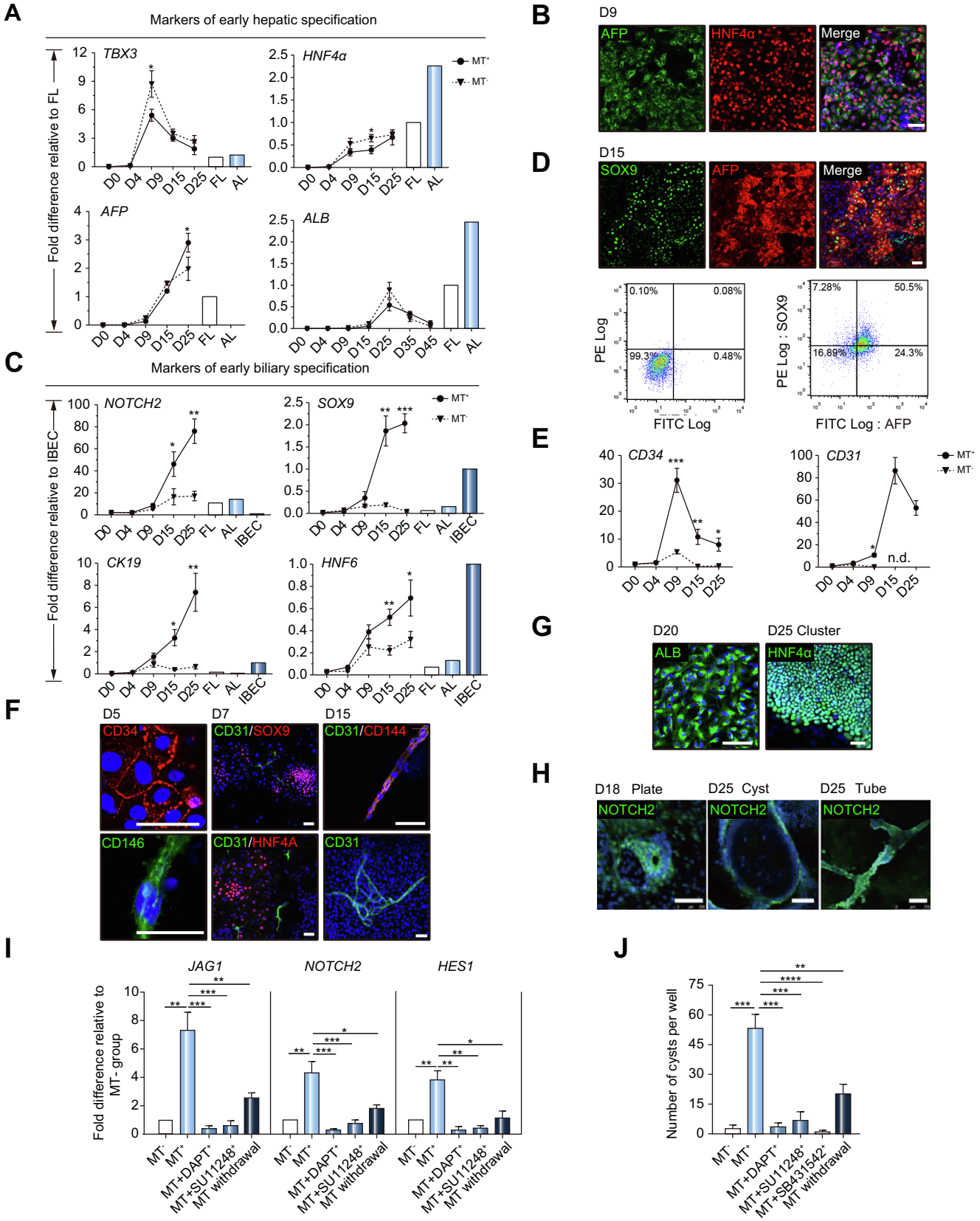
A
Markers of early hepatic specification
Fold difference relative to FL
TBX3
HNF4α
AFP
ALB
MT+
MT-
D0 D4 D9 D15 D25 D35 D45 FL AL
B
D9
AFP
HNF4α
Merge
D
D15
SOX9
AFP
Merge
0.10%
0.08%
99.3%
0.48%
PE Log
FITC Log
7.28%
50.5%
16.89%
24.3%
PE Log : SOX9
FITC Log : AFP
C
Markers of early biliary specification
Fold difference relative to IBEC
NOTCH2
SOX9
CK19
HNF6
D0 D4 D9 D15 D25 FL AL IBEC
E
CD34
CD31
n.d.
G
D20
D25 Cluster
ALB
HNF4α
F
D5
D7
D15
CD34
CD31/SOX9
CD31/CD144
CD146
CD31/HNF4A
CD31
H
D18 Plate
D25 Cyst
D25 Tube
NOTCH2
I
JAG1
NOTCH2
HES1
Fold difference relative to MT- group
MT- MT+ MT+DAPT+ MT+SU11248+ MT withdrawal
J
Number of cysts per well
MT- MT+ MT+DAPT+ MT+SU11248+ MT+SB431542+ MT withdrawal

(Fig. 3B). During the subsequent 6 days, the MT$^+$ group showed rapid upregulation of early biliary specification markers *NOTCH2*, *SOX9*, *CK19* and *HNF6*[21,22] (Fig. 3C). By day 15, all 4 genes in the MT$^+$ group showed significantly higher expression compared to the MT$^-$ group (p <0.05, p <0.01, p <0.05 and p <0.01) (Fig. 3C). During the same period, the expression of hepatic markers in the MT$^+$ group was maintained (*HNF4α*) or continued to increase (*AFP* and *albumin*), and was overall slightly lower than that in the MT$^-$ group by day 15. Moreover, these cells exhibited features of bipotent hepatoblasts, with the co-expression of SOX9 and AFP identified by immunofluorescence and flow cytometry at day 15 (Fig. 3D). These results indicated that bipotent hepatoblast-like cells were generated with more biliary potential in the MT$^+$ group than in the MT$^-$ group.

During liver development, signals from the endothelial lineage promote liver-bud formation[21,23] and guide bile duct morphogenesis.[24] We thus traced mesoderm-derived endothelial lineage in our system. Quantitative PCR analysis showed rapid upregulation of endothelial progenitor marker *CD34* after day 4 and mature vascular endothelial marker *CD31* after day 9 in MT$^+$ group, but persistent low expression was observed in the MT$^-$ group over differentiation (Fig. 3E). Confirmed by immunofluorescence, a small quantity of CD146/CD34-positive cells, and CD31-positive cells in the MT$^+$ group could be identified as early as day 5 and day 7, respectively (Fig. 3F). By day 15, we observed tubular structures that co-stained with CD31 and CD144 over the underlying cells, as well as the CD31-marked tubular network located across the cells. The endothelial differentiation in our system was probably contributed by the combination of Activin A and BMP4 from the differentiation medium, and FGF2 and ascorbic acid from the mTeSR according to several studies on endothelial indcution.[25–27] RNA-Seq profiling of MT$^+$ cells revealed that the genes associated with blood vessel development, extracellular matrix organization, and liver development were highly upregulated at day 15 (ICMJE disclosure). Taken together, these results strongly linked early hepatogenesis and underlined the contribution of 25% mTeSR to model physiologically relevant conditions.

For stage III, we supplemented HCM with OSM and Dex, which is usually used to promote hepatic maturation.[28] A progressive process of hepatic and biliary differentiation in the next 10 days was observed: hepatic cells closely gathered to be clusters (Fig. 3G); in parallel, biliary lineage cells gradually organized into NOTCH2-positive ring-like structures, and then grew into cystic and/or tubular organoids (Fig. 3F). The continued upregulation of hepatic and biliary markers during day 15–25 supported these observations (Fig. 3A and C).

It has been previously shown that NOTCH signaling controls bile duct morphogenesis.[29] As robust upregulation of NOTCH2 was observed in the mTeSR-treated cells (Fig. 3C), we asked whether the NOTCH pathway contributed to the formation of these biliary structures. At day 25, the expression of *NOTCH2*, as well as its ligand *JAG1* and its downstream target *HES1* were significantly increased in the presence of 25% mTeSR (all p <0.01) (Fig. 3I). This increase in expression was reversed by NOTCH signaling inhibitor DAPT (p <0.001, p <0.001, p <0.01) (MT$^+$ DAPT$^+$ in Fig. 3I), resulting in a dramatic reduction in the number of biliary cysts (p <0.001) (Fig. 3J). Consistent with this, mTeSR withdrawal from day 9 led to a constant reduction in all 3 genes (p <0.001, p <0.001, p <0.01) (MT withdrawal in Fig. 3I), with the number of cysts reduced by over a half (p <0.01) (Fig. 3J). These results indicated that 25% mTeSR effectively activated NOTCH signaling, which was required in biliary morphogenesis in this system. However, it seemed that there were no components in mTeSR that could directly activate the NOTCH signaling. Given the fact that NOTCH signaling from vascular endothelial cells controls bile duct morphogenesis,[29] we then investigated whether NOTCH2 was activated by the endogenous signaling from the endothelial-like cells in our system. When the endothelial differentiation was blocked by VEGFR inhibitor SU11248, the expression of JAG1, NOTCH2 and HES1 was all decreased compared with that in the MT$^+$ group (p <0.001, p <0.001, p <0.01) (MT$^+$ SU11248$^+$ in Fig. 3I). In addition, the number of cysts reduced significantly (p <0.001) (Fig. 3J). These results demonstrated that, signaling from hiPSC-derived endothelial-like cells effectively activated NOTCH2, which guided biliary morphogenesis. To validate our hypothesis that TGF-β provided by 25% mTeSR contributed to biliary specification, we performed similar analyses for TGF-β signaling. We blocked the activity of TGF-β with TGF-β inhibitor SB431542 and observed that almost no biliary cysts were formed at day 25 (p <0.0001) (see MT$^+$ SB431542$^+$ in Fig. 3J), which supported our hypothesis. Taken together, these results demonstrated that the biliary specification in our system was dependent on activation of NOTCH and TGF-β signaling by 25% mTeSR.

Hepatic and biliary maturation

During differentiation day 25–35, we observed morphologic deterioration in both hepatic and biliary lineages, and the organoids eventually collapsed upon day 35–45 (data not shown). In

Fig. 3. Hepatic and biliary co-differentiation. (A) Quantitative PCR analysis showed normal, but slightly weaker expression of early hepatic markers over differentiation in the MT+ group when compared with MT− group. FL and AL were used as positive controls. Values are determined relative to *GAPDH* and presented as fold change relative to the expression in FL, which is set as 1. $^*p$ <0.05; n = 3. (B) Immunofluorescence showed the co-expression of AFP and HNF4α in day-9 cells. Scale bars = 50 μm. (C) Quantitative PCR analysis showed significantly higher expression of early biliary markers over differentiation in MT$^+$ group when compared with MT$^-$ group. Human FL, human adult AL and human IBECs were used as controls. Values are determined relative to *GAPDH* and presented as fold change relative to the expression in IBECs, which is set as 1. $^*p$ <0.05, $^{**}p$ <0.01; n = 3. (D) Immunofluorescence showed the co-expression of HNF4α and CK19, and SOX9 and CK19, respectively, in day-15 cells. Scale bars = 100 μm. (E) Quantitative PCR analysis showed the upregulation of endothelial markers in MT$^+$ group. Day-0 hiPSCs was used as negative control. Values are determined relative to GAPDH presented as fold change relative to the expression in day-0 hiPSCs, which is set as 1. $^*p$ <0.05, $^{**}p$ <0.01; n = 3. (F) Immunofluorescence showed the differentiation of hiPSC-derived endothelial lineage. Scale bars = 50 μm. (G) Immunofluorescence showed that albumin-positive hepatocyte-like cells gathered to be large cluster. Scale bars = 50 μm. (H) Immunofluorescence showed that NOTCH2-positive disc structure turned into cystic and/or tubular structure from day 15–25. Scale bars = 50 μm. (I, J) Gain and loss analysis showed that 25% mTeSR contributed to biliary morphogenesis through NOTCH and TGF-β signaling. n = 3. DAPT is a NOTCH signaling inhibitor; SU11248 is a VEGFR inhibitor; SB431542 is a TGF-β signaling inhibitor. MT withdrawal represents that 25% mTeSR was withdrew from day 9. All assays were performed at day 25. MT$^-$ group was used as control. In (I), values are determined relative to *GAPDH* and presented as fold change relative to the expression in MT$^-$ group, which is set as 1. n = 4. In (J), four independent wells were analyzed. n = 4. In (A), (C), (E) (I) and (J), MT$^+$ group represents the protocol that retained 25% mTeSR in differentiation from day 1–15; MT$^-$ group represents the protocol that without mTeSR inclusion. Statistical significance was calculated based on the comparison between MT$^+$ MIX$^+$ and MT$^+$ MIX$^-$ cultures using 2-sided Student's t test. All error bars indicate ± s.d. AFP, alpha-fetoprotein; AL, adult liver; FL, fetal liver; hiPSCs, human induced pluripotent stem cells; IBECs, intrahepatic biliary epithelial cells. (This figure appears in colour on the web.)

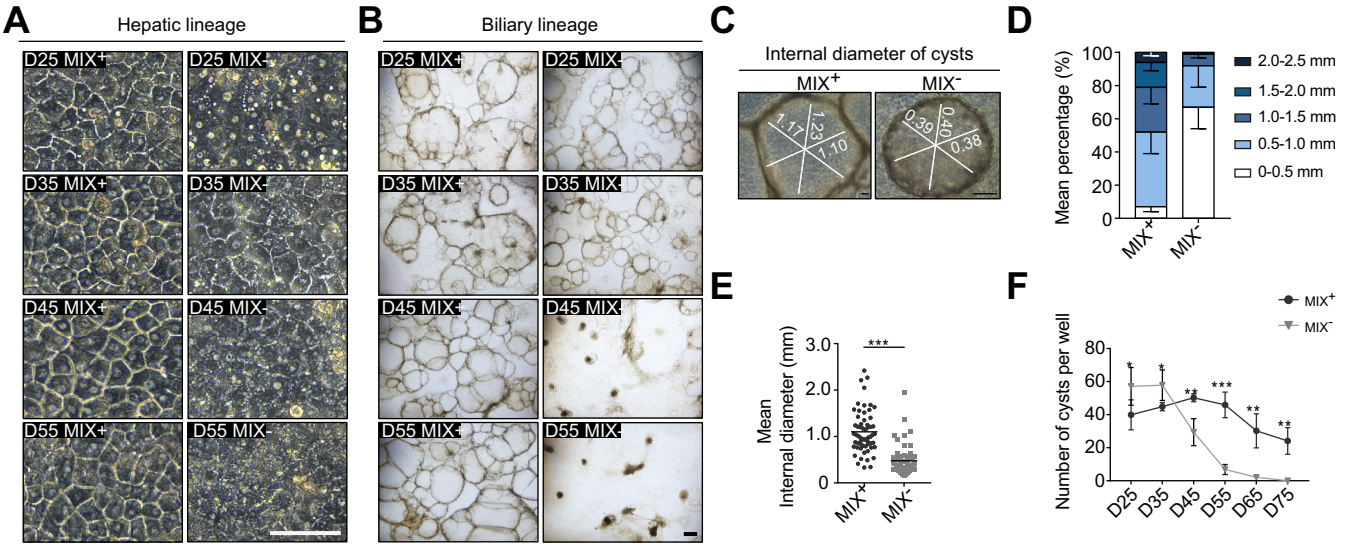

Fig. 4. Cholesterol$^+$ MIX promoted hepatobiliary morphological maturation and facilitates later maintenance. (A, B) Phase-contrast images of hepatic (A) and biliary (shown as cysts, B) lineage of HBOs during day 25–55 with or without Cholesterol$^+$ MIX treatment. Scale bars = 50 μm. (C–E) Mean diameter analysis at day 45 showed significantly larger sizes of the cysts in MIX$^+$ group than those in MIX$^-$ group. Three independent wells with 20 random cysts each were analyzed. Each mean cyst diameter was calculated based on 3 random diameters of the cyst as shown in (B). $^*p$ <0.05, $^{**}p$ <0.01, $^{***}p$ <0.001; n = 3. (F) Number analysis of cysts over differentiation showed slower reduction in the number of cysts in MIX$^+$ group than in MIX$^-$ group. $^*p$ <0.05, $^{**}p$ <0.01, $^{***}p$ <0.001; n = 5. MT$^+$ group represents the protocol that supplemented HCM with Cholesterol$^+$ MIX from day 15; MT$^-$ group represents the protocol that without Cholesterol$^+$ MIX supplement. In (D–F), a 2-sided Student's *t* test was used to calculate statistical significance. All n values represent the number of biological replicates analyzed per condition. All error bars indicate ± s.d. HBOs, hepatobiliary organoids; HCM, hepatocyte culture medium. (This figure appears in colour on the web.)

previous differentiation approaches, *in vitro* maturation of induced hepatocytes were accompanied by accelerated senescence with rapidly decreased function,[30] which might result from the shortage of necessary nutrition and cell-to-cell interaction. Cholesterol was required in developing mammalian cells as it is involved in lipid raft assembly and membrane rigidity maintenance, thus enabling cell membrane signaling.[31–33] Moreover, cholesterol provides building blocks for the synthesis of bile acids.[34] Our uniquely prepared cholesterol$^+$ MIX, which is primarily comprised of cholesterol (15 μg/ml) and other small molecules extracted from Chinese medicine (Fig. S2). We then supplemented HCM with cholesterol$^+$ MIX during stage III (day 15–45) (Fig. 1A). Upon later culture, we observed drastic hepatobiliary morphologic changes between MIX$^+$ or MIX$^-$ groups (Fig. 4). In MIX$^-$ group, significant cell death was observed after day 25. The remaining hepatic cells either became flattened with multiple nuclei (*e.g.*, polykaryons via possible endomitosis), or smaller as if they were undergoing apoptosis (Fig. 4A). The cysts gradually shrunk, becoming small aggregates after day 35, with the number decreasing over culture (Fig. 4B). In contrast, few cells were dead in the MIX$^+$ group. The hepatic cells showed normal morphology and gathered more tightly, with cystic size and number becoming larger and higher, respectively, over culture (Fig. 4C–F). These observations led us to speculate that (i) cholesterol$^+$ MIX might play a role in promoting the hepatic and biliary differentiation/maturation. (ii) cholesterol$^+$ MIX might prevent organoids from senescence.

We then performed several analyses to check the molecular phenotype of day-45 MIX$^+$ hepato-biliary organoids (HBOs) (Fig. 5A). Immunofluorescence analysis identified a large hepatic cluster that consisted of HNF4α-positive hepatocyte-like cells. These cells also expressed CYP3A4, Collagen IV, and albumin that with long tubular endothelial-like cells (marked by CD31) embedded in HBOs (Fig. 5B). Concomitantly, the biliary cysts contained epithelial-like cells that expressed EPCAM, but not albumin (Fig. 5C). They also expressed CFTR with typical bile duct apical–basal polarity and contained primary cilia that were identified by Ac-α-tubulin. These results demonstrated the matured features of hepatocytes and cholangiocytes.

To further validate the effect of MIX in promoting maturity, we examined a series of mature hepatic markers (*albumin*, *AAT*, *HNF4α*, *CYP3A4*, *G6PC* and *TAT*) and biliary markers (*CFTR*, *SSR2*, *ASBT*, *AE2*, *AQP1* and *GGT1*) in HBO with or without MIX treatment (Fig. 5D and E). Quantitative results showed that the upregulation of mature hepatic markers mainly occurred during day 15–35, while the upregulation of matured biliary markers occurred constantly over stage III (day15–45), suggesting that day 45 might be a good timepoint for balancing hepatic and biliary development. It was remarkable that, up to day 45, the expression of almost all of these genes (except for AQP1) in MIX$^+$ HBOs was significantly higher than that in MIX$^-$ HBOs, which was in line with our previous observations (Fig. 4). Besides, we examined the expression of several P450 enzymes and found that day-45 MIX$^+$ HBOs expressed significantly higher *CYP3A4* and *CYP2E1* than fetal liver, with expression of *CYP2A6*, *CYP2B6* and *CYP2D6* comparable to fetal liver (Fig. 5F). Yet, the expression of most of P450 enzymes (except for *CYP3A4*) in HBOs was significantly lower than that in adult liver. Taken together, these results, confirmed by immunofluorescence, supported the role of cholesterol$^+$ MIX in promoting the maturation of HBOs.

Flow cytometry of day-45 HBOs identified about 60% hepatic cells (stained by albumin) and about 32% biliary cells (stained by CK19). The remaining 8% of the cells were not characterized further. The proportion of matured hepatic (stained by CYP3A4) and biliary (stained by CK7) cells is about 48% and 28%, respectively (Fig. 5G).

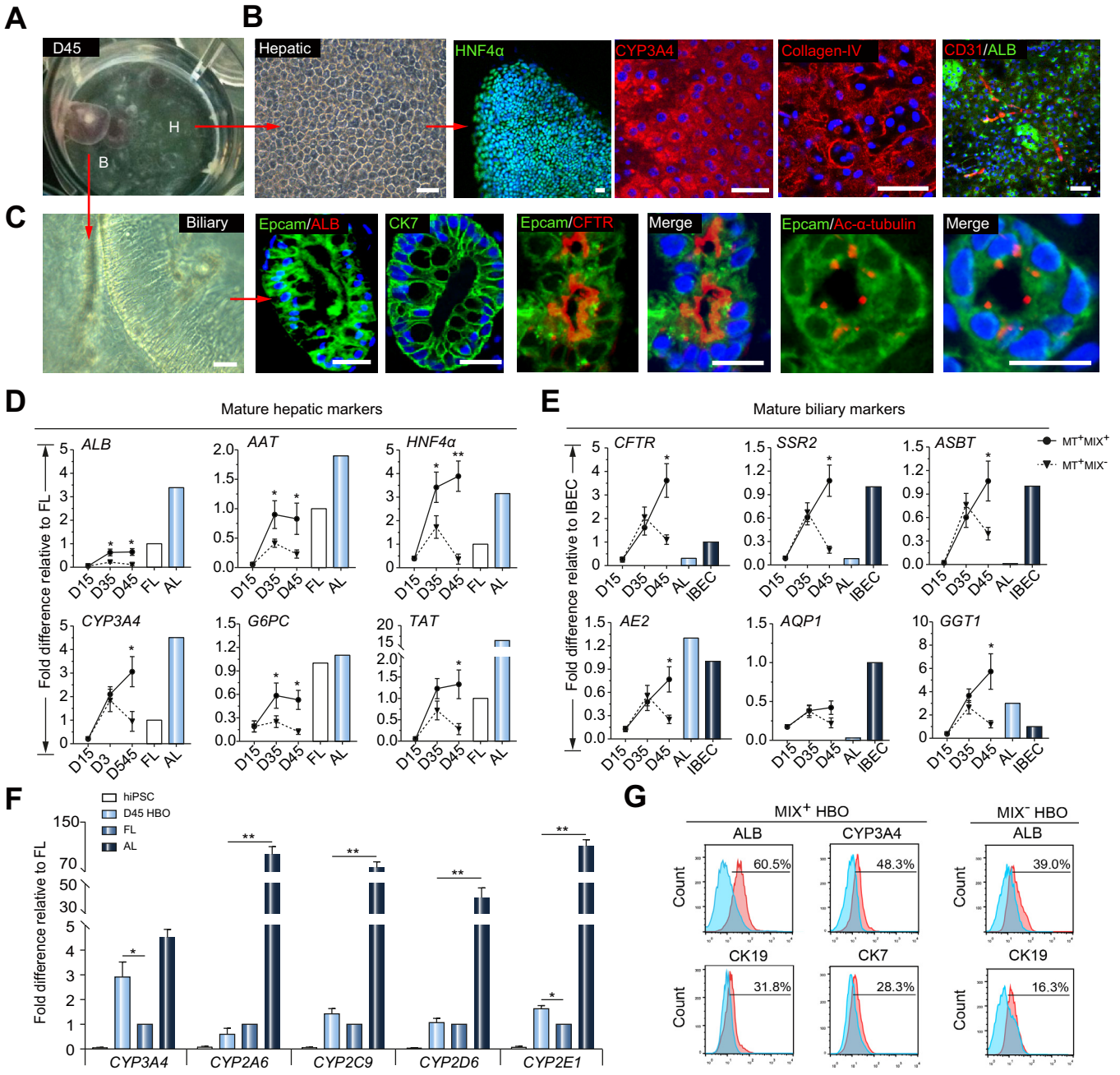

Fig. 5. Cholesterol$^+$ MIX promoted mature phenotype of hepatobiliary organoids. (A-C) Phenotype of day-45 HBO. In (A), "H" represents hepatocyte-like cells; "C" represents cholangiocyte-like cells. Scale bars = 50 μm. (D, E) Quantitative PCR analysis showed that cholesterol$^+$ MIX improved the expression of mature hepatic and biliary markers. In (D), Human FL and human AL were used as positive controls. Values are determined relative to *GAPDH* and presented as fold change relative to the expression in FL, which is set as 1. $^*p$ <0.05; n = 3. In (E), human AL and human IBECs were used as controls. Values are determined relative to *GAPDH* and presented as fold change relative to the expression in IBECs, which is set as 1. $^*p$ <0.05, $^{**}p$ <0.01; n = 3. (F) Quantitative PCR analysis showed that MIX$^+$ HBOs had the expression of several P450 enzymes between fetal liver and adult liver. Day 0 hiPSCs were used as negative control. FL and human AL were used as positive controls. Values are determined relative to *GAPDH* and presented as fold change relative to the expression in FL, which is set as 1. $^*p$ <0.05, $^{**}p$ <0.01; n = 3. (G) Flow cytometry confirmed the proportion of hepatic and biliary lineage cells. In (D–F), a 2-sided Student's *t* test was used to calculate statistical significance. All n values represent the number of biological replicates analyzed per condition. All error bars indicate ± s.d. AL, adult liver; FL, fetal liver; HBOs, hepatobiliary organoids; hiPSCs, human induced pluripotent stem cells; IBECs, intrahepatic biliary epithelial cells. (This figure appears in colour on the web.)

To examine the role of cholesterol$^+$ MIX in anti-senescence, we performed β-Gal staining in HBOs (Fig. 6). Phase-contrast staining images showed less β-Gal+ cells in MIX$^+$ group than those in MIX$^-$ group for both hepatic and biliary cells during differentiation (Fig. 6A). And the observed data showed that cholesterol$^+$ MIX significantly slowed down the senescence of HBOs (Fig. 6B).

Hepatobiliary organoids displayed maturated features

To characterize the function of HBOs, a battery of assays were conducted. PAS staining indicated a glycogen storage function of the hepatic cells (Fig. S3A). The accumulation of fatty droplets was identified by ORO staining (Fig. S3B), indicative of lipid metabolism ability in these hepatocyte-like cells. Moreover, the differentiated hepatocytes were capable of taking up and

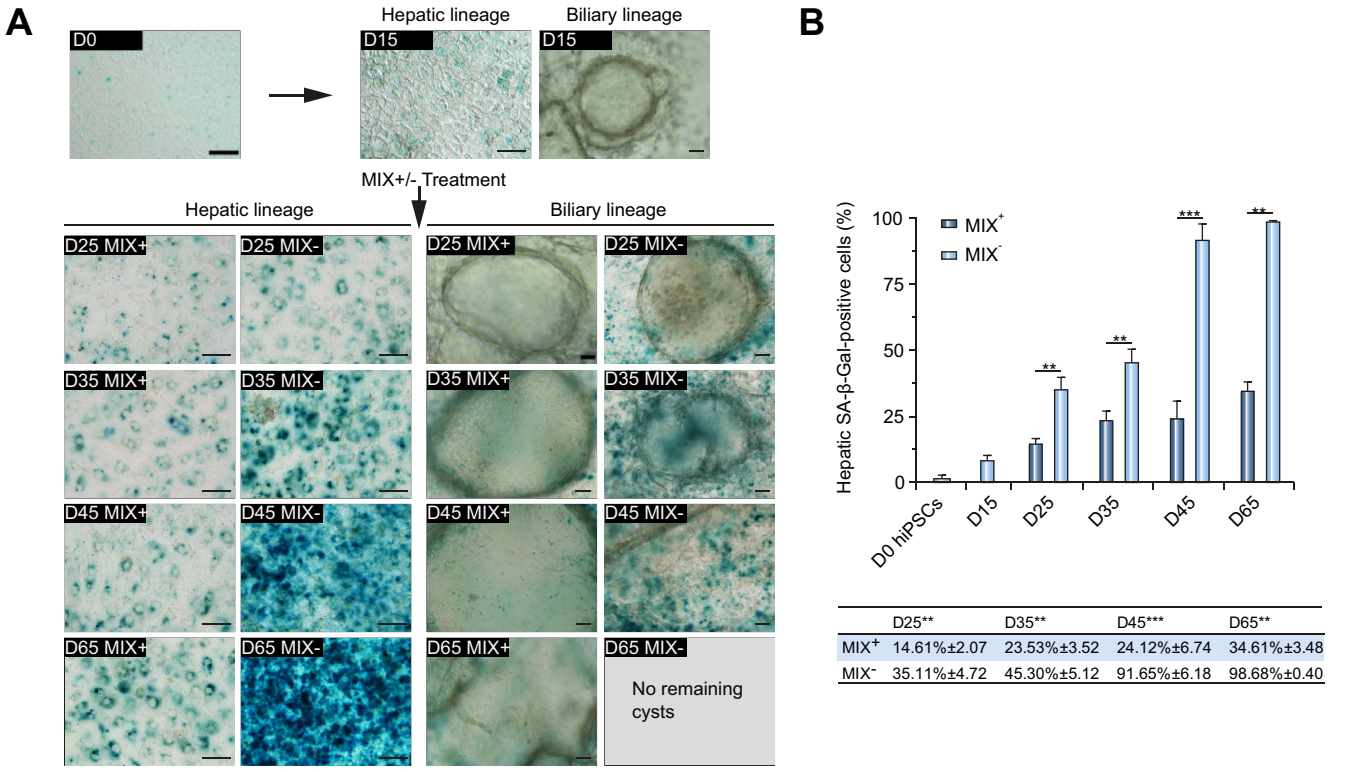

Fig. 6. Cholesterol$^+$ MIX played an anti-senescence role during maturation. (A) Phase-contrast images of senescence β-Gal staining in HBOs during day 25–55 with or without Cholesterol$^+$ MIX treatment. Day 0 hiPSCs and D15 populations were used as controls. Scale bars = 50 μm. (B) Quantification of β-Gal staining showed that Cholesterol$^+$ MIX significantly slowed down hepatocyte senescence. Number of β-Gal-positive cells were quantified by count. n = 3. MT$^+$ group represents the protocol that supplemented HCM with Cholesterol$^+$ MIX from day 15, and MT$^-$ group represents the protocol that without Cholesterol$^+$ MIX supplement. A 2-sided Student's *t* test was used to calculate statistical significance. All n values represent the number of biological replicates analyzed per condition. All error bars indicate ± s.d. HBOs, hepatobiliary organoids; HCM, hepatocyte culture medium; hiPSCs, human induced pluripotent stem cells.

releasing indocyanine green (ICG) (Fig. S3C). Then the AFP, albumin, and urea production of HBOs were assessed (Fig. 7A). Consistent with previous results (Figs. 4 and 5), the MIX$^+$ HBOs showed more durable secretion of albumin and urea when compared with the MIX$^-$ HBOs; and both the MIX$^+$ HBOs showed a secretion delay by 5–10 days compared with monolayer hepatocyte-like cells in MT$^-$ MIX$^-$ group. We then quantified albumin and urea in supernatant of day-35 MT$^+$ MIX$^+$ HBOs and compared this with HepG2 cells and cryopreserved adult human hepatocytes (CAH) (Fig. 7B). The albumin and urea production in day-35 HBOs (5.59 ± 0.86 and 55.41 ± 8.84 μg/ml/day/mg protein) were comparable to those in HepG2 cells (3.47 ± 0.21 and 72.22 ± 7.37 μg/ml/day/mg protein, respectively, p <0.05 and p = 0.07), but were lower than those in CAH (12.27 ± 2.92 and 106.89 ± 15.31 μg/ml/day/mg protein, respectively; p <0.05) when normalized using protein content. Control hiPSCs showed no production of albumin and urea. To evaluate the function of drug metabolism in HBOs, we measured the activity and inducibility of CYP3A4, which mediates the clearance of more than 50% of currently known drugs. Using bioluminescence-based substrates (Promega), CYP3A4 activity in MIX$^+$ HBOs moderately improved over time, reaching the peak of 0.19 ± 0.04 relative light unit/ml/day/mg protein at day 45 of differentiation, comparable to 0.23 × 10 relative light unit/ml/day/mg protein for CAH (Fig. 7C). In contrast, the CYP3A4 activity in MIX$^-$ HBOs dramatically decreased after day 35. Control HepG2 cells showed little CYP3A4 activity. When dosing with either phenobarbital or rifampin (Fig. 7D), day-45 MIX$^+$ HBO demonstrated statistically significant induction (over DMSO-treated control by 1.3–2.7-fold and 1.4–2.8-fold, p <0.05 and p <0.05, respectively); whereas CAH was more robustly induced (1.9–3.3-fold and 2.7–5.5-fold, p <0.01 and p <0.05, respectively).

The secretory potential of cystic structures was confirmed with rhodamine 123, a fluorescent dye used to assess the activity of the multidrug resistance protein-1 (MDR1) in cholangiocytes.[35] As the dye was actively secreted to the luminal space of cysts, the accumulation was prevented by the MDR1 inhibitor verapamil (Fig. 7E), thus it was used to confirm the MDR1-dependent transporter activity. Moreover, day-45 MIX$^+$ HBOs displayed greater GGT activity compared with intrahepatic biliary epithelial cells (p <0.05), and about 10-fold greater activity than MIX$^-$ HBOs, respectively (p <0.001) (Fig. 7F). Notably, bile acid was identified in the lumen of day-45 cyst structures (Fig. 7G), suggesting that the bile acid produced by hepatocytes was transported from bile duct structures to cysts. Taken together, these results indicated that the differentiated hepatocyte-like cells and cholangiocyte-like cells in HBOs had gradually become functionally mature.

Potential of HBO for *in vivo* use

To investigate the potential of HBOs for *in vivo* use, we transplanted HBOs under the splenic capsule of NOD-SCID immune-deficient mice (n = 20) (Fig. 8A).[36,37] Sham operation was performed as control (n = 6). At 4 weeks after transplantation, we identified biliary duct-like structures that stained positive for hCK19 (Fig. 8B), and large hepatic clusters that stained positive for human albumin (Fig. 8C). Little staining was

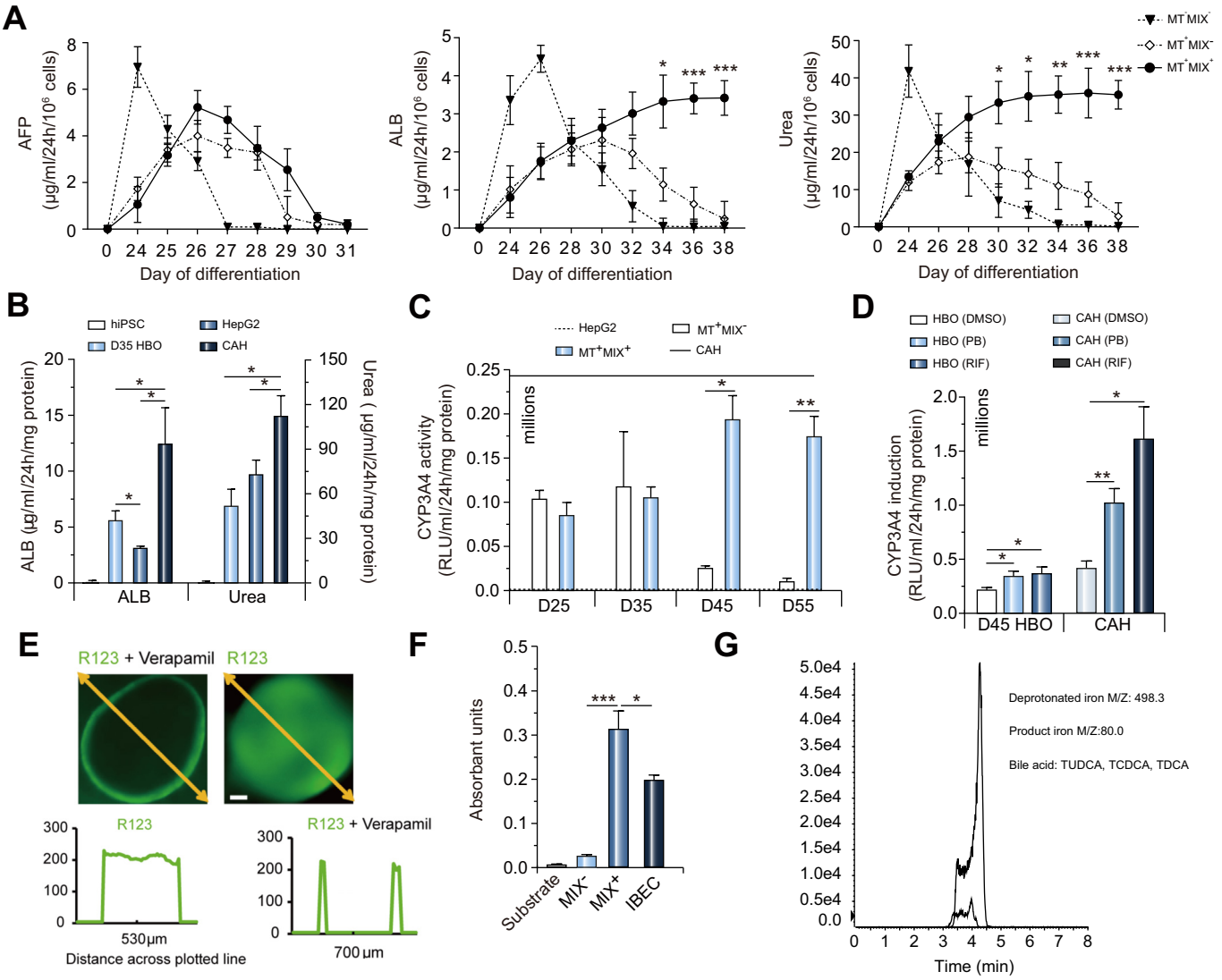

Fig. 7. Functional properties of hepatobiliary organoids. (A) Rate of AFP, albumin and urea secretion during differentiation. *p <0.05; **p <0.01; ***p <0.001; n = 3. MT^- MIX^- and MT^+ MIX^- cultures were used as control. Statistical significance was calculated based on the comparison between MT^+ MIX^+ and MT^+ MIX^- cultures using 2-sided Student's t test. (B) Production of albumin and urea in day-35 HBOs. HepG2 cells and CAHs were used as positive controls; hiPSCs were used as negative control. *p <0.05; **p <0.01; n = 3. (C) Time course of CYP3A4 activity in HBOs with or without Cholesterol$^+$ MIX treatment. CAHs were used as positive control; HepG2 cells were used as negative control. Activity was assessed using bioluminescent assays. The values are indicated as RLU per million cells. *p <0.05, **p <0.01; n = 3. (D) CYP3A4 induction in HBOs. Day-45 HBOs were treated with RIF and PB, followed by assessment of CYP3A4 activity using bioluminescent substrates. CAHs were used as positive control. *p <0.05; n = 4. (E) Representative images demonstrating the MDR1 fluorescent substrate rhodamine 123 detected in the lumen of cystic organoids, confirming MDR1 functionality. Scale bars = 200 µm. (F) GGT activity in day-45 HBOs. Human intrahepatic biliary epithelial cells (IBEC) was used as positive control; Substrate only was used as negative control. n = 4. (G) Identification of bile acids from cysts by LC-MS/MS. In (A–D, F), a 2-sided Student's t test was used to calculate statistical significance. All n values represent the number of biological replicates analyzed per condition. All error bars indicate ± s.d. AFP, alpha-fetoprotein; CAHs, cryopreserved human adult hepatocytes; HBOs, hepatobiliary organoids; hiPSCs, human induced pluripotent stem cells; PB, phenobarbital; RIF, rifampin; RLU, relative light unit. (This figure appears in colour on the web.)

detected in sham-operated spleens confirming the specificity of antibodies. At 8 weeks after transplantation, the biliary structures were well maintained, which was demonstrated by the appearance of hCFTR/Ac-α-tubulin staining with apical–basal polarity (Fig. 8D). But the hepatic structure was not well maintained at 8 weeks, with less human albumin-positive cells identified than in grafts obtained at 4 weeks after transplantation (Fig. 8E). We then found that many of these hepatic cells were in the livers of mice (Fig. 8F). Quantitative results supported these immunofluorescence findings (Fig. 8G).

Teratomas were not found in any of the animals receiving transplants, and the expression of pluripotency markers NANOG and OCT4 was much lower in HBO *in vivo* (8 weeks) than in adult liver (Fig. 8G).

In order to verify these results, we repeatedly induced HBOs with H1 human ES cell lines and iPSC WD lines and obtained the same results consistently (Fig. S4-5).

Discussion

For liver modeling *in vitro*, morphologic and functional maturity has been hampered by the difficulty in mimicking the cellular microenvironment during embryogenesis, that is, the interaction and co-development of various progenitors from multiple germ layers.[38] Given the critical role of mesodermal signals in hepatobiliary development, under the premise of hepatic endoderm differentiation committed by hepatic differentiation mediums, we simultaneously initiated mesodermal differentiation by

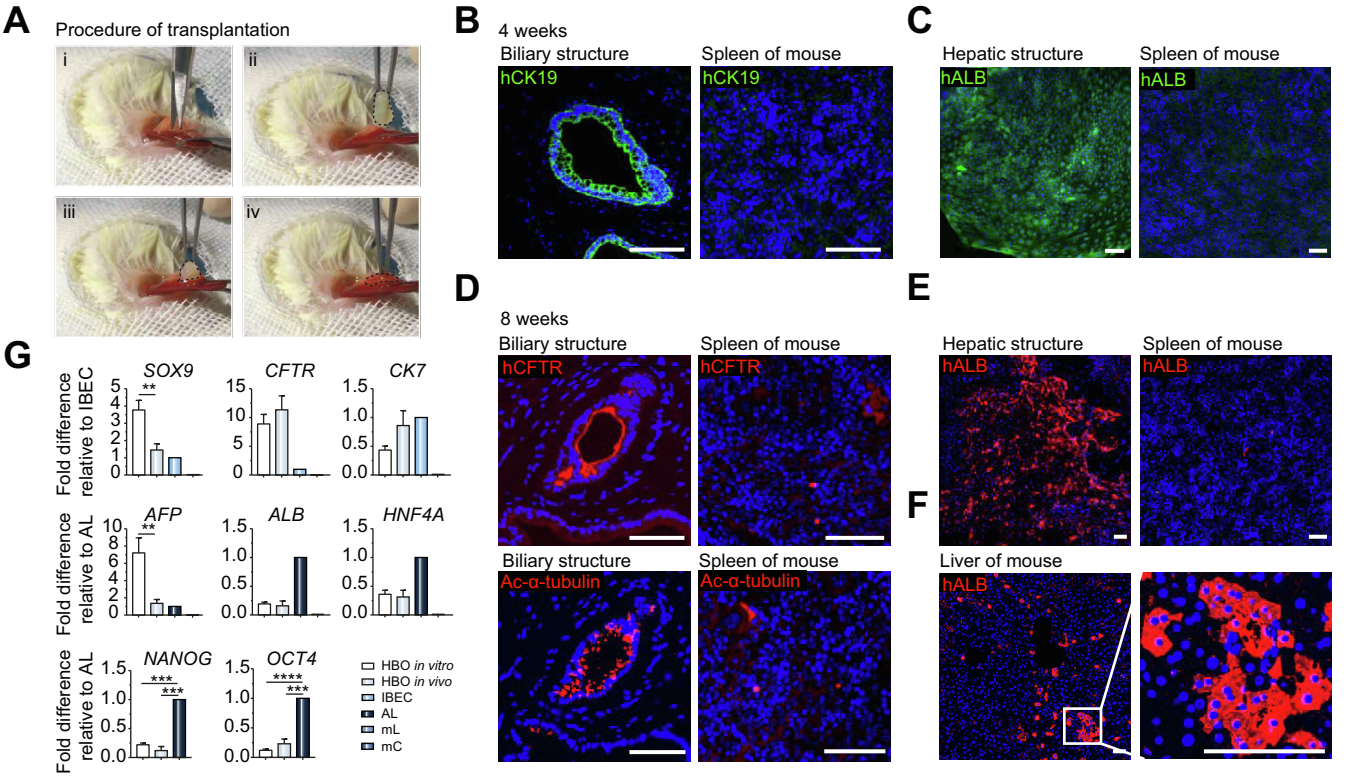

Fig. 8. The engraftment of hiPSC-derived hepatobiliary organoids. (A) The procedure of transplanting HBOs under the splenic capsule. (B, C) Hepatic and biliary structures at 4 weeks of transplantation. The spleens of shame-operated mice were used as negative control. (D, E) Hepatic and biliary structures at 8 weeks of transplantation. The spleens of shame-operated mice were used as negative control. (F) The appearance of engrafted hepatic cells in the liver of mice. (G) Quantitative PCR analysis of hepatic, biliary, and pluripotency markers using human specific primers. HBO *in vitro* represents the cultured day-45 HBO; HBO *in vivo* represents the HBO harvested from the spleens of the mice at the 8 weeks of transplantation. Murine liver or biliary cells was used as negative control; human IBECs or human AL were used as positive controls. Values are determined relative to *GAPDH* and presented as fold change relative to the expression in positive control, which is set as 1. $^{**}p$ <0.01, $^{***}p$ <0.001, $^{****}p$ <0.0001; n = 5. All scale bars = 100 μm. A 2-sided Student's *t* test was used to calculate statistical significance. All error bars indicate ± s.d. AL, adult liver; HBOs, hepatobiliary organoids; hiPSCs, human induced pluripotent stem cells; IBECs, intrahepatic biliary epithelial cells. (This figure appears in colour on the web.)

including 25% mTeSR medium into the protocol, which is one of our key factors in this study. As differentiation proceeded, we observed hepatic, biliary and endothelial differentiation, and obtained HBOs within 4 weeks. Then 10% cholesterol^{+} MIX was utilized to further promote the *in vitro* maturation of HBOs. This is the first study, to the best of our knowledge, to report successful *in vitro* generation of hiPSC-derived 3D functional HBOs, without the need for exogenous cells or genetic manipulation.

The concomitant differentiation of hepatic and biliary lineage in this system to some extent recapitulated several key aspects of early hepatogenesis *in vivo*, including the generation of hepatoblast-like cells and vascular endothelial-like cells, specification of hepatoblast-like cells to hepatocyte and cholangiocyte fate, then the induction and formation of more differentiated hepatocyte-like cells with cystic and tubular structures.

Furthermore, similar to the biliary tubulogenesis in mice, our gain and loss of function analyses demonstrated that the biliary specification in this system was probably co-guided by NOTCH signaling that activated by mesoderm-derived endothelial-like cells, and TGF-β signaling enhanced by mTeSR. These results confirmed the indirect and direct roles of mTeSR in promoting biliary commitment in this system, as well as demonstrating the importance of NOTCH and TGF-β signaling pathways in human cholangiocyte specification. Paralleled with biliary specification, hepatic specification was concomitantly induced. We found the expression of hepatic specific markers in cultures was mildly suppressed compared to the protocol without mTeSR treatment, which might be at the expense of enhanced NOTCH and TGF-β signaling. This led to the delay in AFP/albumin/urea secretion for several days. Nevertheless, a switch from AFP to albumin was also observed in this system, which is one of the stress signs for hepatocyte maturation. By the end of stage (day 45), the HBO was mostly comprised of about 60% hepatocyte-like cells and about 30% cholangiocyte-like cells.

It is important to assess the maturity of HBOs. The typical bile duct apical–basal polarity of matured biliary markers, the presence of primary cilia, together with the ability to transport rhodamine and store bile acid demonstrated a mature phenotype of biliary cells in HBOs. Notably, the HBO displayed more GGT activity than human intrahepatic biliary epithelial cells. Meanwhile, the induced hepatocyte-like cells could take up ICG, store glycogen and accumulate liquid. Expression of P450, the capacity of albumin and urea secretion, CYP3A4 activity and its inductivity in HBOs consistently identified an intermediate maturity between fetal liver and adult liver.

An important aspect of this hepatobiliary system is that there is no requirement for exogenous supportive cells (such as mesenchymal stem cells and fibroblasts),[39–40] liver extracellular matrices[8] or specialized biomaterials,[41,42] thus reducing the experimental variability, costs, and most importantly, the risk of immune-rejection for future transplantation applications.

Recently, liver organoids with biliary structures have been generated by co-culturing with extracellular matrix scaffolds and fetal progenitor cells obtained from human liver tissue.[8] However, human liver tissues are very limited given the scarce availability of suitable donors, and their quality for *in vitro* use varies considerably across different cell types. By contrast, hiPSCs can easily be produced from readily accessible cell types, and hold greater potential to be translated into clinical applications.[43] More importantly, the pattern of producing an organ totally through endogenous cell culture, as shown in our study, is closer to the authentic conditions *in vivo*, thus highlighting the value for future drug development and potential liver transplantation.

To achieve a more matured function of HBOs, it is possible to optimize the current hepatobiliary system based on several considerations: (i) Endogenous signal: the ratio of endoderm and mesoderm might be further optimized by modification of mTeSR concentrations during stage I and II. (ii) Exogenous signal: differentiation studies have underlined the roles of several specific molecules in directing hiPSC-derived hepatoblast-like cells to cholangiocyte-like cells (*e.g.* Activin A, FGF-10 and retinoic acid for TGF-β mediated biliary specification; JAGGED and NOTCH2 for NOTCH pathway mediated tubular morphogenesis).[44–46] Thus, including one or more of these molecules into the current protocol might be useful to enhance the functional of biliary lineage cells in HBO. (iii) Structural support: ECM support has been shown to be critical for *in vitro* hepatic maintenance and differentiation. In this regard, laminin 521/111-based hepatocyte-like cells from hiPSCs were recently reported to achieve higher P450 activity and more robust inducibility compared with those differentiated on Matrigel. Moreover, this matrix also better supported bile canaliculi-like structures in culture. Therefore, laminin matrix seems to be a good candidate for hepatobiliary co-differentiation. Lastly, a 3D approach (*e.g.* matrix overlay) could be attempted to promote maturity by reinforcing the structure and facilitating cellular interactions.[45]

In general, this hepatobiliary system can serve as a tool for developmental and pathological research in the liver, offering more potential to accurately predict drug metabolism and toxicity in future drug development. Besides, the system described herein has enormous therapeutic potential for hepatobiliary system transplantation in end-stage liver failure.

Financial support

This work was supported by the project 2011CB946101 and 2013CB835304 of the National Basic Research Program of China (973) and the project 31871244 of National Natural Science Foundation of China.

Conflict of interest

The authors declare no conflicts of interest that pertain to this work.

Please refer to the accompanying ICMJE disclosure forms for further details.

Authors' contributions

Study concept and design: Anlong Xu and Fenfang Wu; Acquisition of data: Fenfang Wu, Di Wu, Yong Ren, Yuhua Huang; Analysis and interpretation of data: Anlong Xu, Fenfang Wu, Di Wu; Yong Ren; Statistical analysis: Fenfang Wu, Di Wu, Yuhua Huang, Shangwu Chen; Drafting of the manuscript: Fenfang Wu, Di Wu, Yuhua Huang, Yong Ren; Critical revision and final approval of the manuscript: Anlong Xu; Obtained funding: Anlong Xu; Administrative, technical support: Fenfang Wu and Shangwu Chen; Study supervision: Anlong Xu and Fenfang Wu.

Supplementary data

Supplementary data to this article can be found online at https://doi.org/10.1016/j.jhep.2018.12.028.

References

Author names in bold designate shared co-first authorship

[1] Song Z, Cai J, Liu Y, Zhao D, Yong J, Duo S, et al. Efficient generation of hepatocyte-like cells from human induced pluripotent stem cells. CellResearch 2009;19:1233.
[2] **Yang Z**, **Yanxia L**, **Fei Y**, Zhihua S, Han Q, Sha M, et al. Directed differentiation of human embryonic stem cells into functional hepatic cells. Hepatology 2010;45:1229–1239.
[3] **Chen YF**, **Tseng CY**, Wang HW, Kuo HC, Yang VW, Lee OK. Rapid generation of mature hepatocyte-like cells from human induced pluripotent stem cells by an efficient three-step protocol. Hepatology 2012;55:1193–1203.
[4] **Zhao D**, **Chen S**, Duo S, Xiang C, Jia J, Guo M, et al. Promotion of the efficient metabolic maturation of human pluripotent stem cell-derived hepatocytes by correcting specification defects. Cell Res 2013;23:157.
[5] Noto FK, Duncan SA. Generation of hepatocyte-like cells from human pluripotent stem cells. J Vis Exp 2013:139–147.
[6] Lou YR, Leung AW. Next generation organoids for biomedical research and applications. Biotechnol Adv 2017.
[7] Takebe T, Zhang RR, Koike H, Kimura M, Yoshizawa E, Enomura M, et al. Generation of a vascularized and functional human liver from an iPSC-derived organ bud transplant. Nat Protoc 2014;9:396.
[8] **Vyas D**, **Baptista PM**, Brovold M, Moran E, Gaston B, Booth C, et al. Self assembled liver organoids recapitulate hepato-biliary organogenesis in vitro. Hepatology 2017.
[9] Ludwig TE, Levenstein ME, Jones JM, Berggren WT, Mitchen ER, Frane JL, et al. Derivation of human embryonic stem cells in defined conditions. Nat Biotechnol 2006;24:185–187.
[10] Yu P, Pan G, Yu J, Thomson JA. FGF2 sustains NANOG and switches the outcome of BMP4-induced human embryonic stem cell differentiation. Cell Stem Cell 2011;8:326–334.
[11] Weinstein M, Monga SPS, Liu Y, Brodie SG, Tang Y, Li C, et al. Smad proteins and hepatocyte growth factor control parallel regulatory pathways that converge on β1-integrin to promote normal liver development. Mol Cell Biol 2001;21:5122–5131.
[12] Clotman F, Jacquemin P, Plumb-Rudewiez N, Pierreux CE, Van DSP, Dietz HC, et al. Control of liver cell fate decision by a gradient of TGF beta signaling modulated by Onecut transcription factors. Genes Dev 2005;19:1849–1854.
[13] Price KL, Kolatsijoannou M, Mari C, Long DA, Winyard PJD. Lithium induces mesenchymal-epithelial differentiation during human kidney development by activation of the Wnt signalling system. Cell Death Discovery 2018;4:13.
[14] Sullivan GJ, Hay DC, Park I, Fletcher J, Hannoun Z, Payne CM, et al. Generation of functional human hepatic endoderm from human iPS cells. Hepatology 2010;51:329–335.
[15] Zhang W, Yatskievych T, Baker R. Pb. Regulation of Hex gene expression and initial stages of avian hepatogenesis by Bmp and Fgf signaling. Dev Biol 2004;268:312–326.
[16] Sekhon SS, Tan X, Micsenyi A, Bowen WC, Monga SP. Fibroblast growth factor enriches the embryonic liver cultures for hepatic progenitors. Am J Pathol 2004;164:2229–2240.
[17] Hussain SZ, Sneddon T, Tan X, Micsenyi A, Michalopoulos GK, Monga SP. Wnt impacts growth and differentiation in ex vivo liver development. Exp Cell Res 2004;292:157–169.

[18] **Li Q**, **Hutchins AP**, Yong C, Li S, Shan Y, Liao B, et al. A sequential EMT-MET mechanism drives the differentiation of human embryonic stem cells towards hepatocytes. Nat Commun 2017;8:15166.
[19] Suzuki A, Sekiya S, Büscher D, Belmonte JCI, Taniguchi H. Tbx3 controls the fate of hepatic progenitor cells in liver development by suppressing p19ARF expression. Development 2008;135:1589–1595.
[20] Lüdtke THW, Christoffels VM, Petry M, Kispert A. Tbx3 promotes liver bud expansion during mouse development by suppression of cholangiocyte differentiation. Hepatology 2009;49:969–978.
[21] Sitayeb K, Lemaigre FP, Duncan SA. Organogenesis and development of the liver. Dev Cell 2010;18:175–189.
[22] Zong Y, Stanger BZ. Molecular mechanisms of bile duct development. Int J Biochem Cell Biol 2011;43:257–264.
[23] **Matsumoto K**, **Yoshitomi H**, Rossant J, Zaret KS. Liver organogenesis promoted by endothelial cells prior to vascular function. Science 2001;294:559–563.
[24] Aline A, Peggy R, Sabine C, Yiwei Z, François T, Stanger BZ, et al. Intrahepatic bile ducts develop according to a new mode of tubulogenesis regulated by the transcription factor SOX9. Gastroenterology 2009;136:2325–2333.
[25] Orlova VV, Fe VDH, Petrusreurer S, Drabsch Y, Ten DP, Mummery CL. Generation, expansion and functional analysis of endothelial cells and pericytes derived from human pluripotent stem cells. Nat Protoc 2014;9:1514–1531.
[26] Gu M. Efficient differentiation of human pluripotent stem cells to endothelial cells. Curr Protoc Hum Genet 2018;98 e64.
[27] **Bao X**, **Lian X**, Dunn KK, Shi M, Han T, Qian T, et al. Chemically-defined albumin-free differentiation of human pluripotent stem cells to endothelial progenitor cells. Stem Cell Res 2015;15:122–129.
[28] Touboul T, Chen S, To CC, Mora-Castilla S, Sabatini K, Tukey RH, et al. Stage-specific regulation of the WNT/β-catenin pathway enhances differentiation of hESCs into hepatocytes. J Hepatol 2016;64:1315–1326.
[29] Antoniou A, Raynaud P, Cordi S, Zong Y, Tronche F, Stanger B, et al. Intrahepatic bile ducts develop according to a new mode of tubulogenesis regulated by the transcription factor SOX9. Gastroenterology 2009;136:2325–2333.
[30] **Zhou W**, **Hannoun Z**, Jaffray E, Medine CN, Black JR, Greenhough S, et al. SUMOylation of HNF4alpha regulates protein stability and hepatocyte function. J Cell Sci 2012;125:3630–3635.
[31] Krause MR, Regen SL. The structural role of cholesterol in cell membranes: from condensed bilayers to lipid rafts. Acc Chem Res 2014;47:3512–3521.
[32] Mendez AJ, Lin G, Wade DP, Lawn RM, Oram JF. Membrane lipid domains distinct from cholesterol/sphingomyelin-rich rafts are involved in the ABCA1-mediated lipid secretory pathway. J Biol Chem 2001;276:3158–3166.
[33] Porter FD. Human malformation syndromes due to inborn errors of cholesterol synthesis. Curr Opin Pediatr 2003;15:607–613.
[34] Russell DW. The enzymes, regulation, and genetics of bile acid synthesis. Annu Rev Biochem 2003;72:137.
[35] Gigliozzi A, Fraioli F, Sundaram P, Lee J, Mennone A, Alvaro D, et al. Molecular identification and functional characterization of Mdr1a in rat cholangiocytes. Gastroenterology 2000;119:1113–1122.
[36] **Ramanathan R**, **Pettinato G**, Beeston JT, Lee DD, Wen X, Mangino MJ, et al. Transplantation of human stem cell-derived hepatocytes in an animal model of acute liver failure. Surgery 2015;158:349–359.
[37] Raschzok N, Pinkernelle J, Billecke N, Nehls K, Powerski M, Sauer IM, et al. Feasibility of fast dynamic MRI for noninvasive monitoring during ectopic liver cell transplantation to the spleen in a porcine model. Am J Roentgenol 2012;198:1417–1423.
[38] Medvinsky A, Livesey FJ. On human development: lessons from stem cell systems. Development 2015;142:17–20.
[39] Berger DR, Ware BR, Davidson MD, Allsup SR, Khetani SR. Enhancing the functional maturity of induced pluripotent stem cell-derived human hepatocytes by controlled presentation of cell-cell interactions in vitro. Hepatology 2015;61:1370–1381.
[40] Takebe T, Enomura M, Yoshizawa E, Kimura M, Koike H, Ueno Y, et al. Vascularized and complex organ buds from diverse tissues via mesenchymal cell-driven condensation. Cell Stem Cell 2015;16:556.
[41] Medine CN, Lucendo-Villarin B, Storck C, Wang F, Szkolnicka D, Khan F, et al. Developing high-fidelity hepatotoxicity models from pluripotent stem cells. Stem Cells Transl Med 2013;2:505–509.
[42] **Baptista PM**, **Vyas D**, Moran E, Wang Z, Soker S. Human liver bioengineering using a whole liver decellularized bioscaffold. Methods Mol Biol 2013.
[43] Lucendo-Villarin B, Rashidi H, Cameron K, Hay D. Pluripotent stem cell derived hepatocytes: using materials to define cellular differentiation and tissue engineering. J Mater Chem B 2016;4:3433–3442.
[44] Dianat N, Dubois-Pot-Schneider H, Steichen C, Desterke C, Leclerc P, Raveux A, et al. Generation of functional cholangiocyte-like cells from human pluripotent stem cells and HepaRG cells. Hepatology 2014;60:700–714.
[45] Cameron K, Tan R, Schmidt-Heck W, Campos G, Lyall MJ, Wang Y, et al. Recombinant laminins drive the differentiation and self-organization of hESC-derived hepatocytes. Stem Cell Rep 2015;5:1250–1262.
[46] **Ogawa M**, **Ogawa S**, Bear CE, Ahmadi S, Chin S, Li B, et al. Directed differentiation of cholangiocytes from human pluripotent stem cells. Nat Biotechnol 2015;33:853.